Directed self-assembly of nanorod networks: bringing the top down to the bottom up

Directed Self Assembly of Nanorod Networks: Bringing the Top Down to the Bottom Up

Joshua F. Einsle[1], Gunther Scheunert[1], Antony Murphy[1], John McPhillips[2], Anatoly V. Zayats[3], Robert Pollard[1], and Robert M. Bowman[1]

[1] Centre for Nanostructured Media, Queen's University Belfast, Belfast, BT7 1NN, United Kingdom

[2] FEI Company, Europe NanoPort, Achtseweg Noord 5, Bldg, 5651 GG Eindhoven, The Netherlands

[3] Department of Physics, King's College London, Strand, London WC2R 2LS, United Kingdom

E-mail: jeinsle01@qub.ac.uk

Abstract. Self-assembled electrodeposited nanorod materials have been shown to offer an exciting landscape for a wide array of research ranging from nanophotonics through to biosening and magnetics. However, until now, the scope for site-specific preparation of the nanorods on wafers is limited to local area definition. Further there is little or no lateral control of nanorod height. In this work we present a scalable method for controlling the growth of the nanorods in the vertical direction as well as their lateral position. A focused ion beam (FIB) pre-patterns the Au cathode layer prior to the creation of the Anodized Aluminium Oxide (AAO) template on top. When the pre-patterning is of the same dimension to the pore spacing of the AAO template, lines of single nanorods are successfully grown. Further, for sub-200 nm wide features a relationship between the nanorod height and distance from non-patterned cathode can be seen to follow a quadratic growth rate obeying Faradays law of electrodeposition. This facilitates lateral control of nanorod height combined with localised growth of the nanorods.

PACS numbers: 63.22.Gh, 81.16.-c, 81.16.Dn, 81.16.Nd, 82.45.Yz, 81.07.-b

1. Introduction

Nanorods form a particularly interesting class of bottom up nanostructures. With diameters typically of the order of tens of nanometers, and length at least one order of magnitude longer, they provide material properties that are uniquely different from those seen in bulk[1]. Martin and Moskovits pioneered the use of porous anodized aluminium (AAO) templates for the growth of bulk quantities of vertically aligned nanorods[2, 3]. This bottom up approach allows bulk control over the dimensionally of the deposited nanorods through the adjustment of the electrochemical parameters involved in the deposition and anodization processes. The process has been well characterized for both foils[2, 3] and thin films[4]. Both metallic and semiconductor nanorods are demonstrating novel properties in a wide variety of applications including catalytic[5], photovoltaic[6], SERS[7, 8], biosensing[9] and plasmonic wave guiding applications[10].

Most significantly all these applications look at exploiting the properties of nanorods grown *en masse* across an entire substrate or wafer. However, new applications and implementations for nanorods would benefit from being able to control the locality of the growth. Various top down approaches for the localization of nano rod growth in AAO templates have been demonstrated. For example using a focused ion beam (FIB) to selectively close off pores in the AAO templates[11, 12]. Alternately, after growth of the nanorods femtosecond lasers have been used to selectively structure regions in the bulk of the nanorods grown[13]. Both of these approaches provide resolution control at individual pore or nanorod level but suffer from significant disadvantages. The former does not provide height control of nanorods and is not scalable beyond FIB. The latter approach, based on laser ablation, effectively destroys material and is incompatible with microfabrication environments. Further, current fabrication processes produce nanorods where any height variations are not only minimal, but they are distributed across a sample. Consequently an ability to vary the height in a controlled fashion should extend the potential of nanorods and may facilitate further novel physical effects.

Instead of attempting to modify the pores of the AAO template directly, it has been recently shown that the modification of the contact cathode layer used in the electrochemical growth of nanorods results in highly localized regions of growth[14, 15]. This approach demonstrates a successful marriage between top-down and bottom-up fabrication philosophies. In this paper we extend this fabrication approach for the localized growth of nanorods. However, by leveraging the ease of use and spatial resolution of FIB patterning, we are able to examine a question that has not been addressed in any of the previous studies. Namely, we ask, what happens when the patterned structure on the under layer cathode layer is roughly the size of the hexagonal AAO unit cell? Examining the effects of reducing the local size of the electrode is used to provide a theoretical framework for the predictive control and realization of the nanostructures that moves towards repeatable implementation rather than serendipity. Further, by applying the behaviours observed in the patterned cathode features, more complicated nanorod networks are created offering the possibility to form a variety

of new devices based on the use of electro-deposited gold nanorods (GNR) in AAO templates.

2. Experimental Methods

2.1. Fabrication of Localised Nanorods Networks

The fabrication of GNR arrays in thin film AAO templates has been described in depth previously [4]. The base procedure consists of RF sputter depositing an 8nm tantalum pentoxide (Ta_2O_5) adhesion layer, then a 5 nm gold under-layer onto a glass substrate. The Au layer acts as an electrode during the electrodeposition of the GNRs. A 300 nm aluminium layer is next deposited, then anodised to create an array of pores, the size and spacing of which are dependent on anodisation conditions. In the experiments presented here a bulk region of 112.3 mm^2 was anodised. The electrochemical process used resulted in an AAO template with an average periodicity, T, of 68 $\pm$ 7nm and an average pore size, p, of 42 $\pm$ 4 nm. The GNRs are then grown up through the porous alumina matrix through electrodeposition in a controlled manner via real-time monitoring of the longitudinal plasmonic resonance. By depositing for 86 s with an applied voltage of -0.455 V, an average bulk GNR height of 263 $\pm$ 13 nm is achieved. Using the electrodeposition relationships described in section 3 the bulk sheet resistance of the cathode underlayer, R_0, can be determined from the measured experimental parameters.

For this work we carry out the same basic process with a key modification in the procedure; namely, the gold underlayer is now patterned using the focused ion beam of a FEI Nova 600i dual-beam microscope before the deposition of the aluminium film. Subsequent deposition of the aluminium thin film and its anodization creates a porous array as usual. However areas which have had the underlayer removed do not then support the electro-chemical growth of GNRs as is shown in the process flow in figures 1(a) through(f).

To easily verify the controlled growth of GNRs the AAO matrix is chemically removed and imaged with an SEM. As can be observed in figures 2(c) and (d) longer nanorods tend to cluster which is due to capillary effects during the drying procedure as demonstrated by Zhao and Fang [16]. This can be suppressed by growing shorter and thicker wires or resorting to processes like critical point drying.

To successfully pattern the gold layer a high level of control over the ion beam is required to produce successful selective growth. In order to achieve this control, FEI's NanoBuilder package was utilized. This patterning environment supports the use of GDSII photolithography files for the definition of complex geometries, while providing additional tools to control how each of the elements in the pattern are scanned by the ion beam. The scan control implements the advanced patterning strategies pointed out by Hopman *et al*[17]. Application of the suggested spiral scan routine results in patterned regions where the sidewalls are vertical and the bottom of the pattern is planar. This

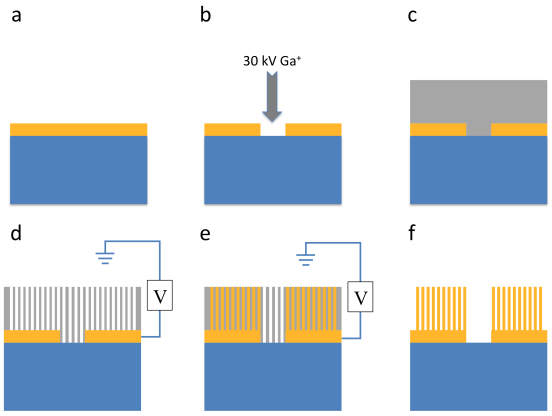

Figure 1. (Color on-line) Schematic of process used to fabricate nanorod networks.(a)Sputter deposition used to deposit Au onto a glass substrate. (b) FIB used to selectively sputter away regions of the Au underlayer. (c) Magnetron sputtering used to deposit Al on the patterned substrate. (d) Pores formed through a process of anodization of the Al layer, forming the AAO matrix. (e) The sample is submerged into a Au solution for electro deposition. (f) Finally, the AAO is removed, leaving the regions of nanorods.

approach insures the complete selective removal of the Au cathode underlayer. Which is critical to insure controlled growth of the GNRs. For the structures fabricated here, beam currents of 28 pA and 93 pA have been selected. The larger beam current allows for efficient removal of large areas of the thin gold underlayer, while the smaller beam current can be effectively used to sputter away smaller regions or perform fine trimming routines. A further restriction on the patterning capability of the FIB comes not from the ion beam it self but rather from the material that the ion beam is sputtering away. In the case of the polycrystalline gold forming the contact electrode, the various grain sizes and boundaries provide the ultimate limit on the how smooth an edge can be formed. Through careful control of patterning parameters however, this roughness is on the order of 10 nm.

To explore the growth dynamics introduced by restriction of the cathode bridge size, the first structure fabricated is a sequence of cathode bridges with various widths ranging from 500 nm down to 30 nm. A top down SEM image of these bridges pre-GNR growth is shown in figure 2(a). Further, growth dynamics are explored through the joining of multiple cathode bridges of various widths. One demonstration of this can be seen in figure 5(a).

2.2. Characterization of GNR Growth

In order to resolve the height of the grown GNRs, the sample was tilted to 52° with respect to the SEM. By tilting the sample the 3D nature of the nanorods can be observed, where as top down images only allow for resolution of the spacing and rod diameter.

The series of straight cathode bridges Employing the high resolution stage on the Dual Beam system allows the for sequential imaging of 1.2 μm fields of view along the contact bridge. Using this sequential imaging technique, a sampling of the individual GNR's in the micrograph are then measured manually using the microscopes annotation software. The software automatically corrects for tilt in the image. Both the height and the distance from the bulk edge of the bridge are recorded. These micrographs can then be stitched together to provide high magnification imagoes showing the nanorod growth dynamics along an individual cathode bridge. This process is repeated for all of the resolution contact bridges fabricated. The data collected is then used to build the electrodeposition growth model described below.

3. Results and Discussion

The focus of this work examines the interplay between the local cathode layer geometry (and thus its resistivity) and the resulting ability for the cathode to support growth of nanorods. Of particular interest is the question of what happens when the patterned cathode bridge width starts to match the dimensional spacing of the pores in the AAO template. This effect is first demonstrated in the 'resolution' grating shown in figures 2(a) and (b). The device fabricated employs the use of the FIB to fashion a series of 12 μm long nanobridges of various widths in the gold cathode layer. As noted in section 2.1, the FIB offers a direct and fast way to create a wide range of nanostructures. This offers a convent method to explore the fundamental growth dynamics of interest, while providing an approach which can be up-scaled through the lithographic approaches.

On these cathode bridges the nanowires have electrochemically grown in the AAO template using the parameters described above. To fully explore the dynamics, these cathode bridge widths run from 500 nm at the widest down to 30 nm. This range of bridge explores the growth on contact cathodes which range from ten unit cells down to a region smaller than a single unit cell. The SEM micrograph in figure 2a shows a resolution grating selectively patterned into the cathode under layer using the FIB. While figure 2b shows the same structure after the electrodeposition of GNR and the chemical removal of the AAO template. For line widths below 150 nm there is a noticeable reduction in the rod height as the rods move to the centre of the under layer cathode bridge . This becomes especially pronounced in all the sub-100 nm wide lines. Figures 2c and 2d, show a photomontage of the 70 nm bridge. This cathode bridge was chosen since it is the first one to become discontinuous in the centre. In becoming discontinuous the 70 nm cathode bridge demonstrates that the ability to support growth is a function of not only the width of the bridge, but also the distance along the bridge that a particular nanorod is displaced from the bulk media. Further, figure 3 is a micrograph of 50 nm cathode bridge width. This width yields effectively a single row of GNR growth. In some places the line width goes to two rods wide, but this arises from the AAO pores being arranged in a hexagonal array. An identical effect can be seen on the 30 nm line, but due to the rapid decrease in rod height the effect is less

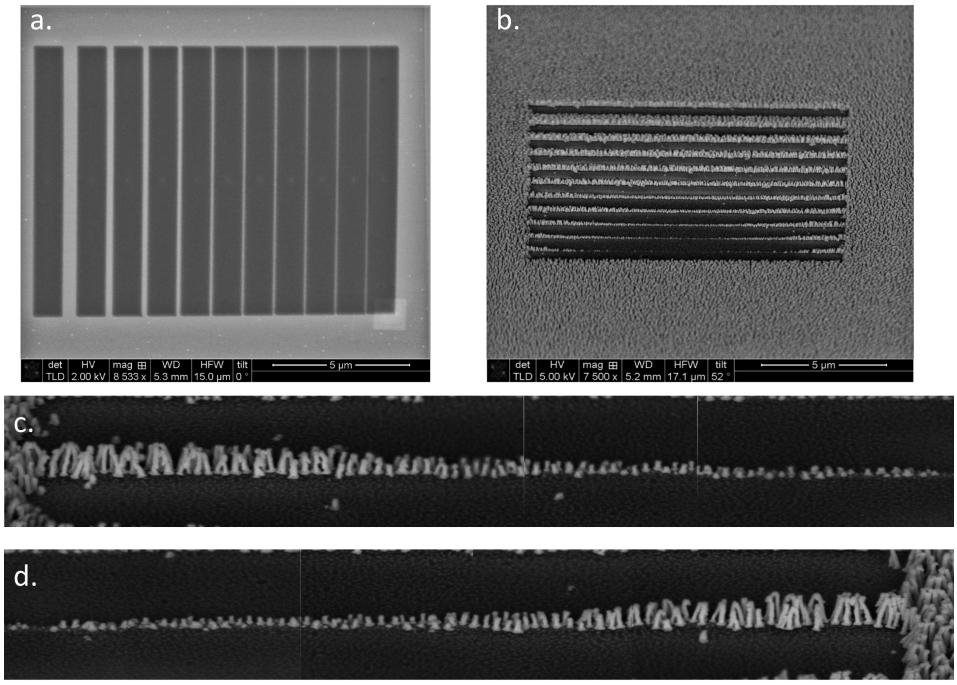

Figure 2. A resolution grating structure showing various line widths achieved using the fabrication technique.(a)Top down image of pre-patterned Au electrode before GNR growth. (b) Micrograph of resolution grating structure rotated 90° and tilted 52° from the top down SEM image to reveal GNR height profiles along the various line widths. (c) The left half of 70 nm grating line photomontage demonstrating decreasing height profile as the line moves away from bulk media. (d) The right half of the 70 nm grating line demonstrating how height is improved moving back towards the bulk of sample.

pronounced. For both the 30 nm and 50 nm cathode bridge s the ability to support growth as a function of displacement from the bulk cathode becomes further amplified over the 70 nm case.

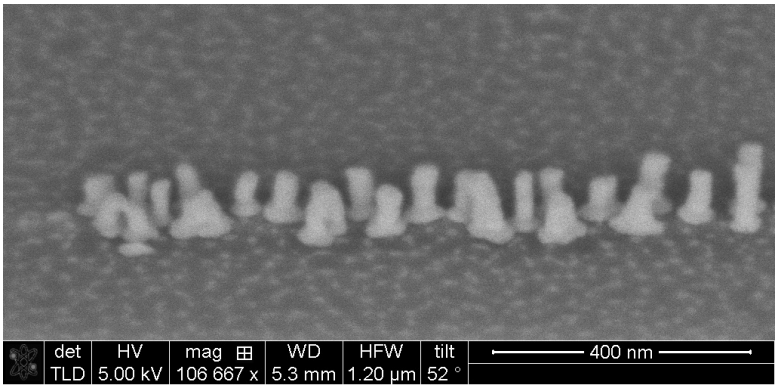

Figure 3. Detail from 50 nm cathode bridge showing minimal line width, with the periodicity of the anodization array.

Phenomenologically, the growth properties shown in the grating device can be understood by recognizing that as the underlayer cathode bridge s become narrower, and a GNR's position moves further from the bulk 'sheet' resistance of the main underlayer to positions of increased resistance. Reviewing the electrodeposition growth mechanics of nanorods into AAO templates will provide a verification of this instinctive understanding.

From the original studies of electrodeposition Faraday derived a relationship between the amount of material deposited and the total charge delivered to a sample in a fixed time,

$$Q(t) = n(t)ZF, \tag{1}$$

where Q is the overall charge, n is the amount of substance depoitsed, Z is the ionic number [18], F is the Faraday constant[19]. We restate (1) so that a relationship of the nanorod height can be determined from the growth parameters of applied voltage U_0, the pore density of the AAO matrix and the chemical properties of gold ions. First by re-expressing the deposited amount $n(t)$ in terms for the mass density,ρ_m[20], the molar mass, M_{mol}[21], and the deposited volume of gold,$V(t)$, as:

$$Q(t) = \frac{\rho_m V(t)}{M_{mol}} ZF. \tag{2}$$

Realizing that the volume deposited, is a time dependant filling of the AAO pores. The volume then becomes a function of the rod height, $h(t)$ and the area of the anodized sample occupied by the pores. The ratio between the surface of the nanorod pores A_p and the entire sample surface A_{sample} is referred to as the porosity, P. By assuming that the pores arrange into a perfect hexagonal array of perfectly cylindrical nanopores, P can be described by geometrical relationship[22]:

$$P = \frac{A_p}{A_{sample}} = \frac{\pi}{2\sqrt{3}} \left(\frac{p}{T}\right)^2, \tag{3}$$

where p describes the average pore diameter, and T gives the average inter-nanorod spacing. Using (3) to find A_p as a function of the overall sample area and the AAO template parameters, allows for the rewriting of (2) into a form that describes the deposition time dependent length of the nanorods. This new relationship is given as:

$$h(t) = \frac{2\sqrt{3}\, M_{mol}}{\pi\, Z\, F\, \rho_m\, A_{sample}} \left(\frac{T}{p}\right)^2 Q(t). \tag{4}$$

The only remaining quantity in the above relation not explicitly stated in terms of experimental parameters is the amount of charge applied during the deposition of the gold ions. Recognizing that the total charge is the definite integral of the applied current with respect to time allows for the substitution of $Q(t)$ with

$$Q(t) = \alpha \frac{|U_0|}{R_0} t, \tag{5}$$

where R_0 is the resistance of the gold underlayer and U_0 is the voltage used during the electrodeposition process. It is important to mention that the integral of the current-vs-time profile measured during the deposition process is not equal to the deposition charge, $Q(t)$. Polarisation effects taking place at the initial deposition stage result in an observed minima in the deposition curve during the nanorod growth. Due to these losses the actual charge is smaller than the change calculated from the current over a fixed period of time. Further, the process of pore creation in the AAO does not actually produce perfectly cylindrical cavities, with perfect hexagonal arrangement. Previous studies have demonstrated that these effects are accounted for by using an empirical current efficiency α of 0.9[23, 24].

Substituting this description of the charge using in the growth process into (4), allows for the following description of bulk rod height as a function of the experimental parameters,

$$h(t) = \alpha \frac{2\sqrt{3}\, M_{mol}}{\pi\, Z\, F\, \rho_m\, A_{sample}} \left(\frac{T}{p}\right)^2 \frac{|U_0|}{R_0} t. \tag{6}$$

Using the experimental conditions outlined in section 2.1 and the measured bulk GNR height of 263 $\pm$ 13 nm this relationship is then used to determine the sheet resistance of the cathode under layer,R_0.

When we seek to apply the above relation to predict $h(t)$ along a cathode bridge a local model of the resistivity is required. A single cathode bridge connected at both ends to the bulk cathode layer presents a local region where the overall volume of gold is reduced, resulting in a nanostructure with a higher resistivity than than bulk cathode. To realise this we choose a model that treats each rod with an equivalent circuit model whereby cathode bridges are represented by two parallel resistors. An cathode bridge connected at only one end to the bulk cathode layer will still support growth. However, from the basic definition of resistivity since this isolated gold cathode bridge has a reduced area and finite length, its resistivity will be higher than the rest of the bulk contact layer. In this way the cathode bridge becomes a resistor with respect to the circuit completed by a GNR growing on in the electrochemical bath. By connecting the cathode bridge at both ends to the bulk cathode layer, a single GNR along the bridge will experience a resistance from both sides. The picture for the impedance experienced by a single GNR then is one of two parallel resistors connected to a bulk resistance. Analytically, this means that in (6) R_0 will be replaced by,

$$R = R_0 + \frac{R_p \cdot R_s}{R_p + R_s}, \tag{7}$$

where R_p and R_s are the resistances from each end of the connected bridge experienced by a GNR at a particular position l along the cathode bridge. From the basic definition of resistivity, the resistances for the left and right sides of the bridge can

be given as,

$$\begin{aligned} R_p(l) &= \rho_s \frac{l}{A_b} \\ R_s(l) &= \rho_s \frac{L_b - l}{A_b}. \end{aligned} \tag{8}$$

The overall length of the bridge is L_b. Assuming a constant rectangular cross section for the cathode bridge, A_b, is the under layer thickness times the width of the bridge. The bulk resistivity of gold is used for ρ_s[20]. Using (8), combined with (7) the growth model along a cathode bridge now becomes,

$$h(t) = \alpha \frac{2\sqrt{3}\ M_{mol}}{\pi\ Z\ F\ \rho_m\ A_{sample}} \left(\frac{T}{p}\right)^2 \frac{|U_0|}{R_0 + \frac{\rho_s}{A_b} \cdot \frac{l}{L_b}(L_b - l)} t. \tag{9}$$

Using the measurement routine described in section 2.2, collection of nanorod height along several of the cathode bridge widths is summarised by the black dotted lines in figures 4(a) through (f). It should be noted that the non-symmetric position of the minima in the collected growth curves arises from the accumulation stage move errors during the measurement process. While these contribute to slightly skewed curve shapes they do not significantly alter the analysis of the growth mechanism. This same figure shows the application of the parallel resistor model as indicated by the dotted red curve.

Examination of the measurement data for cathode bridge widths below 100 nm shows the simple parallel resistor model does not fully account for the growth dynamics. The grating device shown in figure 2, was fabricated using a 28 pA beam which has a quoted FWHM beam diameter of 17 nm. So for very narrow structures the beam tails on both sides of the cathode bridge start to interact and sputter away excess amounts of Au. For thicker cathode bridges, this effect transforms the cross-section from a simple rectangle into a trapezoidal shape. This tapering is a well know artefact of FIB patterning, and can be minimized through scan strategies[17]. These strategies though can not fully minimize ion beam tail effects when the gold bridge width becomes less than a few ion beam diameters wide. At this point depending on the amount of time that each side of bridge is patterned to remove the bulk cathode layer, the cross section shape of a bridge will take on one of several geometries in a cyclic process. Through the sputtering of the bridge material the cross-section will evolve from a trapezoid to a triangle and then back into a trapezoid with an overall lower height. This process of over milling becomes minimized once the cathode bridge widths are greater than a 100 nm. For these wide cathode bridges the original parallel resistor model becomes the better fit.

One method to include this experimental consequence for narrow cathode bridge s is to create a description of the cross sectional area which varies as the distance from the bulk media. Such a function is given by,

$$A_b^{eff}(l) = A_b \cdot \left(1 - \phi \frac{l(L_b - l)}{L_b^2}\right). \tag{10}$$

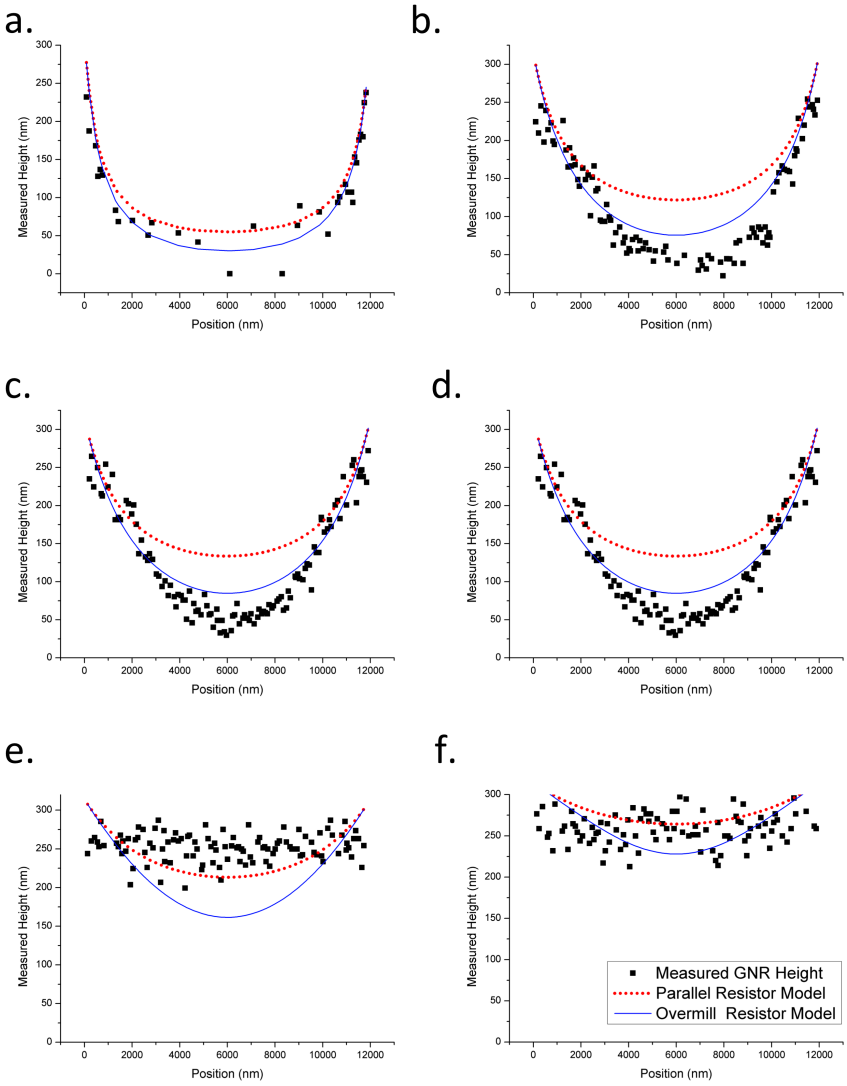

Figure 4. Measured GNR heights for various nano bridge widths. Red curves represent the fit of parallel resistor model. The blue curve illustrates the fit results for a modified cross-sectional area of the nano-bridge. a) GNR results for 30 nm cathode bridge. b) 60 nm wide cathode bridge. c) 70 nm wide cathode bridge. d) 100 nm wide cathode bridge. e) GNR cathode bridge width of 200 nm. f) 500 nm wide cathode bridge.

Here ϕ is a parameter describing the amount of over milling seen on a cathode bridge. It varies from zero for a perfect square cross-section to four for a bridge which has been completely sputtered away in patterning. The blue curves plotted in figure 4, represent a ϕ value of 2.5. This approach accounts for the fact that as pattern moves away from the bulk, the only material the FIB can interact with is the small region defining the cathode bridge. These arguments are further strengthened by measuring the cathode bridge widths with a top down high resolution SEM imaging. Since these images show that the mean cathode bridge width is the specified fabrication dimension,

any change in the cross-sectional area comes initially from sputtering away material from the cathode bridge.

For the 200 nm wide cathode bridge, figure 4(e), and the 500 nm wide bridge, figure 4(f), the parallel resistor model again becomes the better fit. However, it can be observed the measured data has a much more linear shape than suggested by the model. It should be noted the average GNR heights are still below the bulk rod height of 263 ± 13 nm. This shows that for cathode bridges above 100 nm wide the conductivity becomes more bulk like in nature, but a noticeable increase in the cathode bridge resistivity can still be observed and partially accounted for by the parallel resistor model.

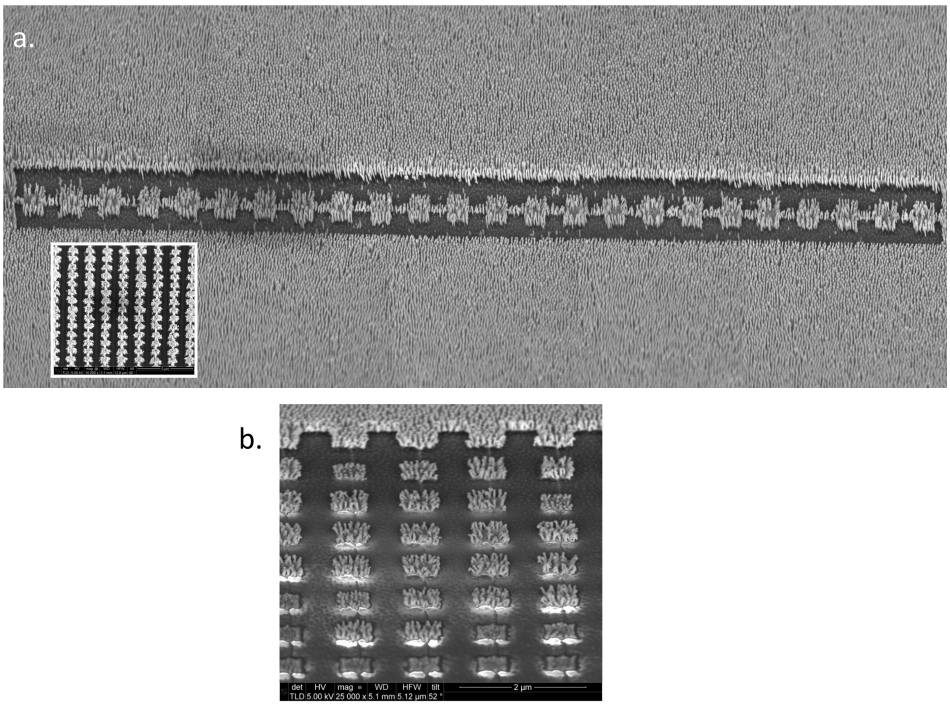

Figure 5. a) A micrograph photomontage of 30 micron long nanorod network of various cathode bridge widths. By initiating the pattern with a narrow channel current is driven through the structure, allowing for continuous growth for the entire length. Photomontage is composed of five images, each with a horizontal field width of 6 μm. Linking together multiple chains results in arrays of islands seen in the inset. b) Islands are formed by connecting 500 nm by 500 nm cathode pads with 30 nm wide cathode bridges.

With our above understanding and by combining the observed dynamics for different bridge widths, it now becomes possible to create several networks of nanorod growth with ultimately result in localized growth of islands of GNR.

First, by stitching together regions of differing cathode bridge widths, a saw tooth like pattern is formed as seen in figure 5(a). This structure stretches for 30 μm and closer inspection reveals that there is a uniform rod height throughout the structure. It is then possible to extend this to larger arrays such as arranging multiple chain patterns

into a square array, a 30 μm by 30 μm grid can be formed as illustrated in the inset of figure 5(a).

We observe that using the FIB for the pattering of the Au underlayer one can achieve remarkably clean and clear edge definition of the structure created. Areas where there are missing rods in the pattered regions, seen in figure 5(a) are due either to rods being lost with the removal of the AAO template or rods that have been lost through repeated imaging with the SEM.

These first two examples show the basic idea for creating an array of isolated islands of GNR growth. Figure 5(b) shows a detail from an array where the connecting under layer bridge has been reduced to the 30 nm limit. In this case growth along the cathode line has been fully inhibited, but growth on the pads is still permitted. This illustration provides as second insight into how the dynamics of GNR growth can be controlled. Within several periods the islands in figure 5(b) start to demonstrate a significant reduction in rod height. This can be understood by first comparing the initial structure outside of the bulk in this case is a 500 nm wide pad. In comparison the uniform growth shown in figure 5(a) results from starting the structure with a narrow cathode bridge . These two contrasting behaviours confirm that a narrow cathode bridge exhibits higher resistivity than possessed by a wider one. Thus, by starting with a higher resistance (i.e. a narrow cathode bridge) the deposition current is driven through the chain pattern in the under layer allowing for uniform growth. Conversely, when a GNR chain is started with a pad structure the resistivity of the narrow bridges is too high to allow the flow of current through the entire structure. By combining these behaviours it should be possible to build even more complex nanorod networks than the ones presented here. One such new application would be in the construction of magnetic plasmonic devices as suggested in the recent work by Liu *et al*[25] and Stashkevich *et al*[26]. By being able to control the locality of GNR growth magneto-plasmonic wave guiding should be possible. Further, coupling into spin waves should be possible by growing nanorods from magnetically interesting metals as suggested by the current magnonics research[27]. Since the electrochemical growth of nanorods is not limited to metallic rods, using nanoscale patterned electrodes opens up the application of this fabrication approach to a wide range of applications in semiconductor, and nanotechnology[1, 6, 28].

4. Conclusion

We have demonstrated that through the combination of top down FIB patterning of the cathode layer with the bottom up growth of GNR in AAO templates, fundamental electrochemical growth mechanisms can be addressed. Importantly, by selectively patterning the cathode with structures, which are scaled to match the pore spacing of the AAO template, we are now able to control both the density of GNR growth as well as the height laterally. Significantly we have developed a formalism to predictably design features that will reduce the density of GNRs down to single elements. Additionally, GNR height is shown to be a function of cathode bridge width and distance from the

bulk cathode layer. It has been demonstrated that creating fine gold cathode lines to larger structures isolated growth can be achieved. By periodically connecting cathode bridges that do not support growth to larger cathode bridges, it is possible to construct extended single rows of GNR growth. The combined power of top down structuring of the gold cathode layer with the scalability of AAO grown nanorods, new device applications beyond the ones discussed in the introduction can be envisaged.

References

[1] Guozhong Cao and Dawei Liu. Template-based synthesis of nanorod, nanowire, and nanotube arrays. *Advances in Colloid and Interface Science*, 136(1–2):45 – 64, 2008.

[2] C.R. Martin. Nanomaterials - a membrane-based synthetic approach. *Science*, 266(5193):1961–1966, DEC 23 1994.

[3] D Routkevitch, T Bigioni, M Moskovits, and JM Xu. Electrochemical fabrication of cds nanowire arrays in porous anodic aluminum oxide templates. *Journal Of Physical Chemistry*, 100(33):14037–14047, AUG 15 1996.

[4] P Evans, W R Hendren, R Atkinson, G A Wurtz, W Dickson, A V Zayats, and R J Pollard. Growth and properties of gold and nickel nanorods in thin film alumina. *Nanotechnology*, 17:5746–5753, 2006.

[5] Yang Yu, Krishna Kant, Joe G. Shapter, Jonas Addai-Mensah, and Dusan Losic. Gold nanotube membranes have catalytic properties. *Microporous And Mesoporous Materials*, 153:131–136, MAY 1 2012.

[6] Punniamoorthy Ravirajan, Ana M. Peiró, Mohammad K. Nazeeruddin, Michael Graetzel, Donal D. C. Bradley, James R. Durrant, and Jenny Nelson. Hybrid polymer/zinc oxide photovoltaic devices with vertically oriented zno nanorods and an amphiphilic molecular interface layer. *The Journal of Physical Chemistry B*, 110(15):7635–7639, 2006. PMID: 16610853.

[7] Matthew D. Doherty, Antony Murphy, John McPhillips, Robert J. Pollard, and Paul Dawson. Wavelength dependence of raman enhancement from gold nanorod arrays: Quantitative experiment and modeling of a hot spot dominated system. *The Journal of Physical Chemistry C*, 114(47):19913–19919, 2010.

[8] Michael Stenbæk Schmidt, Jörg Hübner, and Anja Boisen. Large area fabrication of leaning silicon nanopillars for surface enhanced raman spectroscopy. *Advanced Materials*, 24(10):OP11–OP18, 2012.

[9] John McPhillips, Antony Murphy, Magnus P. Jonsson, William R. Hendren, Ronald Atkinson, Fredrik Höök, Anatoly V. Zayats, and Robert J. Pollard. High-performance biosensing using arrays of plasmonic nanotubes. *ACS Nano*, 4(4):2210–2216, 2010. PMID: 20218668.

[10] Gregory A. Wurtz, Robert Pollard, Willam Hendren, G. P. Wiederrecht, D. J. Gosztola, V. A. Podolskiy, and Anatoly V. Zayats. Designed ultrafast optical nonlinearity in a plasmonic nanorod metamaterial enhanced by nonlocality. *Nature Nanomaterials*, 6:107–111, 2011.

[11] N.-W. Liu, A. Datta, C.-Y. Liu, C.-Y. Peng, H.-H. Wang, and Y.-L. Wang. Fabrication of anodic-alumina films with custom-designed arrays of nanochannels. *Advanced Materials*, 17(2):222–225, 2005.

[12] Nai-Wei Liu, Chih-Yi Liu, Huai-Hsien Wang, Chen-Feng Hsu, Ming-Yu Lai, Tung-Han Chuang, and Yuh-Lin Wang. Focused-ion-beam-based selective closing and opening of anodic alumina nanochannels for the growth of nanowire arrays comprising multiple elements. *Advanced Materials*, 20(13):2547–2551, 2008.

[13] C. Reinhardt, S. Passinger, B. N. Chichkov, Wayne Dickson, Gregory A. Wurtz, Paul Evans, Robert Pollard, and Anatoly V. Zayats. Restructuring and modification of metallic nanorod arrays using femtosecond laser direct writing. *Applied Physics Letters*, 89:231117, 2006.

[14] Alexandru Vlad, Maria Matefi-Tempfli, Vlad A. Antohe, Sebastien Faniel, Nicolas Reckinger,

Benoit Olbrechts, Andre Crahay, Vincent Bayot, Luc Piraux, Sorin Melinte, and Stefan Matefi-Tempfli. Nanowire-decorated microscale metallic electrods. *Small*, 4(5):557–560, 2008.

[15] Dieter Weber, Yulia Mourzina, Dorothea Brueggemann, and Andreas Offenhauesser. Large-scale patterning of gold nanopillars in a porous anodic alumina template by replicating gold structures on a titanium barrier. *Journal of Nanoscience and Nanotechnology*, 11(2):1293–1296, 2011.

[16] Y.-P. Zhao and J.-G. Fan. Clusters of bundled nanorods in nanocarpet effect. *Applied Physics Letters*, 88:103123, 2006.

[17] Wico C L Hopman, Feridun Ay, Wenbin Hu, Vishwas J Gadgil, Laurens Kuipers, Markus Pollnau, and Rene M de Ridder. Focused ion beam scan routine, dwell time and dose optimizations for submicrometre period planar photonic crystal components and stamps in silicon. *Nanotechnology*, 18:1–11, 2007.

[18] T Inoue, S Ando, H Okudaira, J Ushio, A Tomizawa, H Takehara, T Shimazaki, H Yamamoto, and H Yokono. Stable non-cyanide electroless gold plating which is applicable to manufacturing of fine pattern printed wiring boards. In *45TH ELECTRONIC COMPONENTS & TECHNOLOGY CONFERENCE - 1995 PROCEEDINGS*, PROCEEDINGS - ELECTRONIC COMPONENTS AND TECHNOLOGY CONFERENCE, pages 1059–1067, 345 E 47TH ST, NEW YORK, NY 10017, 1995. IEEE, Components Packaging & Mfg Technol Soc; Electr Ind Assoc, I E E E.

[19] W. Vielstich. *Elektrochemie*. Wiley-VCH Verlag, 2005.

[20] Peter Wilkinson. Understanding gold plating. *Gold Bulletin*, 19:75–81, 1986. 10.1007/BF03214646.

[21] D. R. Lide, editor. *CRC handbook of chemistry and physics*, volume 1. CRC Press/Taylor and Francis Group, Boca Raton, Florida, 73 edition, 1992.

[22] K Nielsch, J Choi, K Schwirn, RB Wehrspohn, and U Gosele. Self-ordering regimes of porous alumina: The 10% porosity rule. *Nano Letters*, 2(7):677–680, JUL 2002.

[23] Shan Guan and Bradley J. Nelson. Electrodeposition of low residual stress conimnp hard magnetic thin films for magnetic mems actuators. *Journal of Magnetism and Magnetic Materials*, 292(0):49 – 58, 2005.

[24] G Riveros, S Green, A Cortes, H Gomez, RE Marotti, and EA Dalchiele. Silver nanowire arrays electrochemically grown into nanoporous anodic alumina templates. *Nanotechnology*, 17(2):561–570, JAN 28 2006.

[25] Na Liu, Shaunak Mukherjee, Kui Bao, Yang Li, Lisa V. Brown, Peter Nordlander, and Naomi J. Halas. Manipulating magnetic plasmon propagation in metallic nanocluster networks. *ACS Nano*, 6(6):5482–5488, 2012.

[26] A. A. Stashkevich, Y. Roussigné, P. Djemia, S. M. Chérif, P. R. Evans, A. P. Murphy, W. R. Hendren, R. Atkinson, R. J. Pollard, A. V. Zayats, G. Chaboussant, and F. Ott. Spin-wave modes in ni nanorod arrays studied by brillouin light scattering. *Physical Review B*, 80(14):144406, October 2009.

[27] A. V. Chumak, P. Pirro, A. A. Serga, M. P. Kostylev, R. L. Stamps, H. Schultheiss, K. Vogt, S. J. Hermsdoerfer, B. Laegel, P. A. Beck, and B. Hillebrands. Spin-wave propagation in a microstructured magnonic crystal. *Applied Physics Letters*, 95(26):262508, 2009.

[28] Shunfeng Li and Andreas Waag. Gan based nanorods for solid state lighting. *Journal of Applied Physics*, 111:071101, 2012.